THE JOURNAL OF BIOLOGICAL CHEMISTRY
Vol. 278, No. 12, Issue of March 21, pp. 10675–10682, 2003

Printed in U.S.A.

Binding of the Anticonvulsant Drug Lamotrigine and the Neurotoxin Batrachotoxin to Voltage-gated Sodium Channels Induces Conformational Changes Associated with Block and Steady-state Activation*

Received for publication, August 15, 2002, and in revised form, November 8, 2002
Published, JBC Papers in Press, November 12, 2002, DOI 10.1074/jbc.M208356200

Nora B. Cronin‡, Andrias O'Reilly‡§, Hervé Duclohier¶, and B. A. Wallace‡‖

From the ‡Department of Crystallography, Birkbeck College, University of London, London WC1E 7HX, United Kingdom and ¶Unité Mixté de Recherche 6026 CNRS-Université de Rennes I, Laboratoire des Interactions Cellulaires et Moléculaires, Campus de Beaulieu, Batiment 13, 35042 Rennes Cedex, France

Voltage-gated sodium channels are dynamic membrane proteins characterized by rapid conformational changes that switch the molecule between closed resting, activated, and inactivated states. Sodium channels are specifically blocked by the anticonvulsant drug lamotrigine, which preferentially binds to the channel pore in the inactivated open state. Batrachotoxin is a lipid-soluble alkaloid that causes steady-state activation and binds in the inner pore of the sodium channel with overlapping but distinct molecular determinants from those of lamotrigine. Using circular dichroism spectroscopy on purified voltage-gated sodium channels from *Electrophorus electricus*, the secondary structures associated with the mixture of states present at equilibrium in the absence of these ligands were compared with specific stabilized states in their presence. As the channel shifts to open states, there appears to be a significant change in secondary structure to a more α-helical conformation. The observed changes are consistent with increased order involving the S6 segments that form the pore, the domain III–IV linker, and the P-loops that form the outer pore and selectivity filter. A molecular model has been constructed for the sodium channel based on its homology with the pore-forming regions of bacterial potassium channels, and automated docking of the crystal structure of lamotrigine with this model produces a structure in which the close contacts of the drug are with the residues previously identified by mutational studies as forming the binding site for this drug.

Voltage-gated sodium channels play an important physiological role in excitable membranes, underlying action potential initiation and propagation in nerves and muscles (1). They are also involved in a number of pathophysiologies, *e.g.* rhythm dysfunctions in the heart (2), and channelopathies (3, 4) due to inherited mutations, including hyperkaleimic periodic paralysis, myotonia congenita, and Long QT syndrome. Although their functions have been extensively characterized via electrophysiology (5), structural studies remain scanty, and the molecular basis of the central process of gating is still elusive despite recent progress (6).

Sodium channels show strong sequence conservation across species and tissue-specific types (7). The sodium channel from the electric eel electroplax is 60% identical with that of voltage-gated sodium channels from human muscle. The patterns of hydrophobicity and homologous residues are even more closely preserved, and this indicates that their three-dimensional structures will be very similar. The primary structure of the sodium channel from *Electrophorus electricus* was deduced from its cDNA sequence (8) and revealed the protein to consist of 1820 amino acids, producing a molecular mass of 208 kDa. There are also extensive sugar moieties covalently linked to the protein on its external face, making the total molecular mass of the channel ~260–270 kDa (9). Its sequence contains four highly homologous internal repeats (domains I–IV), each of which consists of six transmembrane–spanning segments (S1–S6), plus linking regions of differing lengths between the domains and extended aqueous-soluble N- and C-terminal domains.

The intracellular linker between domains III and IV has been identified by mutation studies (10) as being involved in fast inactivation, and an NMR study of this peptide in isolation (11) suggested that it has the potential for folding as an α-helix. The C-terminal intracellular domain has also been associated with a form of inactivation and a postulated interaction with the N-terminal segment; its secondary structure has been analyzed by circular dichroism (CD)[1] spectroscopy (12, 13). The S4 transmembrane segments from domains I–IV have been identified as the main voltage sensors (14), whereas the S5–S6 segments and the intervening P-loop regions from domains I–V include residues comprising the transmembrane pore-associated helices and the ion selectivity filter (15).

The low resolution (19 Å) three-dimensional structure of the sodium channel from *E. electricus* determined by cryoelectron microscopy and single particle image analysis (16) revealed an overall architecture of four domains with pseudo-4-fold symmetry surrounding a central pore. The molecule is bell-shaped with an extracellular domain and transmembrane domain together comprising ~50% of the total volume and a large intracellular domain occupying the remaining volume.

* This work was funded by Project Grant B15499 from the Biotechnology and Biological Sciences Research Council (BBSRC) (to B. A. W.), a joint travel grant from the Royal Society and the CNRS (to B. A. W. and H. D.), and an equipment grant from the CNRS (to H. D.). The circular dichroism instrumentation was supported, in part, by Grant B14225 from the BBSRC (to B. A. W.). The costs of publication of this article were defrayed in part by the payment of page charges. This article must therefore be hereby marked "*advertisement*" in accordance with 18 U.S.C. Section 1734 solely to indicate this fact.

§ Supported by the British Heart Foundation H. W. Fletcher Ph.D. Studentship.

‖ To whom correspondence should be addressed. Tel.: 44-207-631-6857; Fax: 44-207-631-6803; E-mail: ubcg25a@mail.cryst.bbk.ac.uk.

[1] The abbreviations used are: CD, circular dichroism; LTG, lamotrigine; BTX, batrachotoxin; NRMSD, normalized root mean square deviation; TTX, tetrodotoxin; pS, picosiemens.

The sodium channel can adopt distinct but correlated functional conformational states during resting, activation, inactivation, and deactivation. A conformational change upon voltage activation allosterically modifies the conformation of the transmembrane pore, which is spatially separate from the voltage sensors (17). The sodium channel acts as a capacitor in that there is a time lag between stimulation and opening of sodium gates. The stimulus charges the channel over a period of time leading to a conformational change or sequence of conformational changes of the sodium channel protein, which effectively opens the gate initiating an ionic current.

Neurotoxins and drugs such as local anesthetics, anticonvulsants, and antiarrhythmics that modify sodium channel function have been shown to bind preferentially to specific conformational states affecting either activation, inactivation, or both (for a review, see Ref. 18). The antiepileptic drug lamotrigine (LTG) binds preferentially to open sodium channels during inactivation with apparent pore block (19). Batrachotoxin (BTX) binds preferentially to the open state causing steady-state activation (20), prevents all forms of inactivation, and slows deactivation. LTG and BTX bind to specific sites that have been shown by mutagenesis to have overlapping but distinct molecular determinants in the S6 transmembrane segments of domains I, III, and IV (19). Ligand binding appears to be facilitated by gating movements of the pore segments allowing access to their binding sites (21).

To investigate the structural nature of the different functional states of the sodium channel, we have used LTG and BTX to shift the equilibrium mixture of states normally present in the absence of ligands to one of the specific functionally defined conformational states. CD spectroscopy was used to examine conformational changes associated with binding of these ligands to the sodium channel purified from *E. electricus*. These studies have shown that when either lamotrigine or batrachotoxin binds there is a significant change in secondary structure.

MATERIALS AND METHODS

Genapol C-100 (10% solution) was obtained from Calbiochem. IgM anti-α-2,8 *N*-acetylneuraminic acid was extracted from horse antiserum, a gift from Dr. R. Schneerson of the NICHD (22). Lamotrigine was a gift from Dr. R. W. Janes, Queen Mary College, University of London. Batrachotoxin was a gift from Dr. J. W. Daly of the NIDDK. Polyacrylhydrazido-agarose, lipids, protease inhibitors, and rabbit anti-horse IgG were purchased from Sigma. CNBr-activated Sepharose 4B Fast Flow and PHAST gels were from Amersham Biosciences and polyvinylidene fluoride membranes were from BDH Laboratory Supplies.

Isolation and Solubilization of Electroplax Membranes

Membranes were purified from frozen electroplax tissue in a manner similar to that previously described (23, 24) but with a number of modifications designed to increase the yield and maintain protein integrity: thawed diced tissue was suspended in 5 volumes of buffer A (200 mM NaCl, 10 mM sodium phosphate buffer, pH 7.4, 5 mM EDTA, 1 mM EGTA, 0.1 mM phenylmethylsulfonyl fluoride, 0.025% pepstatin, 0.025% leupeptin, 0.025% aprotinin, 0.02% NaN_3) and homogenized at 20,000 rpm for 1 min. After filtration, the sample was centrifuged at 4000 $\times$ *g* for 30 min. The pellets were resuspended in 5 volumes of buffer A, and the homogenization, filtration, and centrifugation steps were repeated. The pellets were resuspended in the buffer at a concentration of 1.5 mg/ml and stored at −80 °C. Membrane yield was ~20% of original electroplax tissue weight.

Solubilization of proteins from electroplax membranes was achieved by addition of Genapol C-100 to the membrane suspension, resulting in a final detergent concentration of 2%. The suspension was homogenized and centrifuged at 100,000 $\times$ *g* for 1 h at 2 °C. The supernatant contained solubilized electroplax membranes.

Immunoaffinity Chromatography Purification of Sodium Channels

IgM was purified from an ammonium sulfate precipitate using an affinity column of polyacrylhydrazido-agarose resin. Purified IgM was coupled to CNBr-activated Sepharose 4B as previously described (24) at ratios of 1.35 mg of IgM per ml of resin. The IgM affinity resin was equilibrated with buffer B (50 mM sodium phosphate buffer, pH 7.4, 0.1% Genapol C-100, 0.2 mg/ml egg phosphatidylcholine, 5 mM EDTA, 1 mM EGTA, 0.1 mM phenylmethylsulfonyl fluoride, 0.025% pepstatin, 0.025% leupeptin, 0.025% aprotinin). The solubilized electroplax membrane fraction was bound to the resin for 2 h. The protein was eluted using a linear gradient of buffer B supplemented with 3.0 M KCl. The eluted fractions were concentrated in a pressure ultrafiltration cell (Amicon) with a PBMK 300K membrane (Millipore).

Reconstitution into Liposomes and Mixed Lipid Micelles

For electrophysiology studies, the sodium channel was reconstituted into liposomes by dialysis of the protein solution (concentration ~ 50 μg/ml) overnight against 1 liter of 150 mM sucrose, 0.5 mM $MgCl_2$, 0.1 M Tris, and 25 mM HEPES, pH 7.4, using a Spectra/Por membrane (molecular mass cut-off, 100 kDa). For CD spectroscopy, the protein was dialyzed against 20 mM sodium phosphate buffer containing 0.1% Genapol C-100 to produce lipid/detergent mixed micelles.

Characterization of Purified Channels

SDS-Polyacrylamide Gel Electrophoresis and Western Blot Analyses—The solubilized and purified protein fractions were examined by SDS-polyacrylamide gel electrophoresis after the method of Laemmli (25). The gel was calibrated using standards ranging from 53 to 220 kDa. The 4–15% gradient PHAST acrylamide gels were silver-stained (26), or the protein was electrotransferred to a polyvinylidene difluoride membrane. For Western blot analysis, the primary antibody was an aliquot of the purified anti-sialic acid horse IgM. The secondary antibody was rabbit anti-horse IgG conjugated to alkaline phosphatase.

Protein Concentration Determination—The relative protein concentrations were determined with the bicinchoninic acid assay (27) using bovine serum albumin as the standard. The bicinchoninic acid analysis was calibrated for the absolute sodium channel protein concentration via duplicate quantitative amino acid analyses of the channel protein.

Single-channel Conductance in Planar Lipid Bilayers—For single channel conductance studies, planar lipid bilayers were formed using the tip-dip method, (28) *i.e.* at the tip of a patch-clamp pipette. A 1-ml Teflon chamber and the patch pipette were filled with electrolytic solution (0.5 M NaCl, 10 mM HEPES buffer, pH 7.4, sterile filtered through 22 μm). The pipette solution, equivalent to the *cis*-side of the bilayer, was supplemented with 1 μM BTX. Ag/AgCl electrodes were employed in the bath and pipette.

Bilayers were formed using the droplet technique, where 20 μl of a bacterial phosphatidylethanolamine/bovine phosphatidylserine/egg phosphatidylcholine (5:4:1) lipid solution (1 mg/ml in hexane) were applied to the micropipette shank just dipping at the air-salt solution interface. A triangular voltage waveform of amplitude ~20 mV and frequency ~100 Hz was applied to check capacitance values after bilayer formation. After checking bilayer stability and electrical silence under applied voltage, 20 μl of ~50 μg/ml reconstituted sodium channels were added to the bath, *i.e.* the *trans*-side. The pipette electrode was connected to the patch-amplifier through a preamplifier or headstage with a 1-giga-ohm resistor (or gain). The sampling rate was 3 kHz, and the low-pass Bessel filter was set at 300 Hz during data acquisition.

Electron Microscopy—Aliquots of samples to be used for CD spectroscopy were applied at a protein concentration of ~50 μg/ml to carbon-coated copper grids and stained with 2% (w/v) uranyl acetate. These were then examined with a TECNAI 1200Ex transmission electron microscope operating at 120 kV.

Circular Dichroism Spectroscopy—The CD spectra were obtained using an Aviv 215 spectropolarimeter, which was specially modified to have a large angle detection geometry (≥90 degrees) for scattering samples such as membrane proteins (29). The instrument was calibrated with camphor sulfonic acid for optical rotation and benzene vapor for wavelength. Data were collected at 0.2-nm intervals, at a constant temperature of 25 °C over a wavelength range from 300 to 185 nm. Five scans were collected for each protein sample and baseline (consisting of the dialysate), and all samples were recorded in the same 0.02-cm pathlength Suprasil cuvette. The averaged baseline spectrum was subtracted from the averaged sample spectrum, and the net spectrum smoothed with a Savitsky-Golay filter (30). Measurements were only made down to wavelengths where the instrument dynode voltage indicated that the detection was still within the linear range.

The sodium channel protein (0.53 μM) was examined in the presence and absence of ligands, either lamotrigine (50 μM) or BTX (1.5 μM). To each sample, ligand dissolved in ethanol was added to produce a final

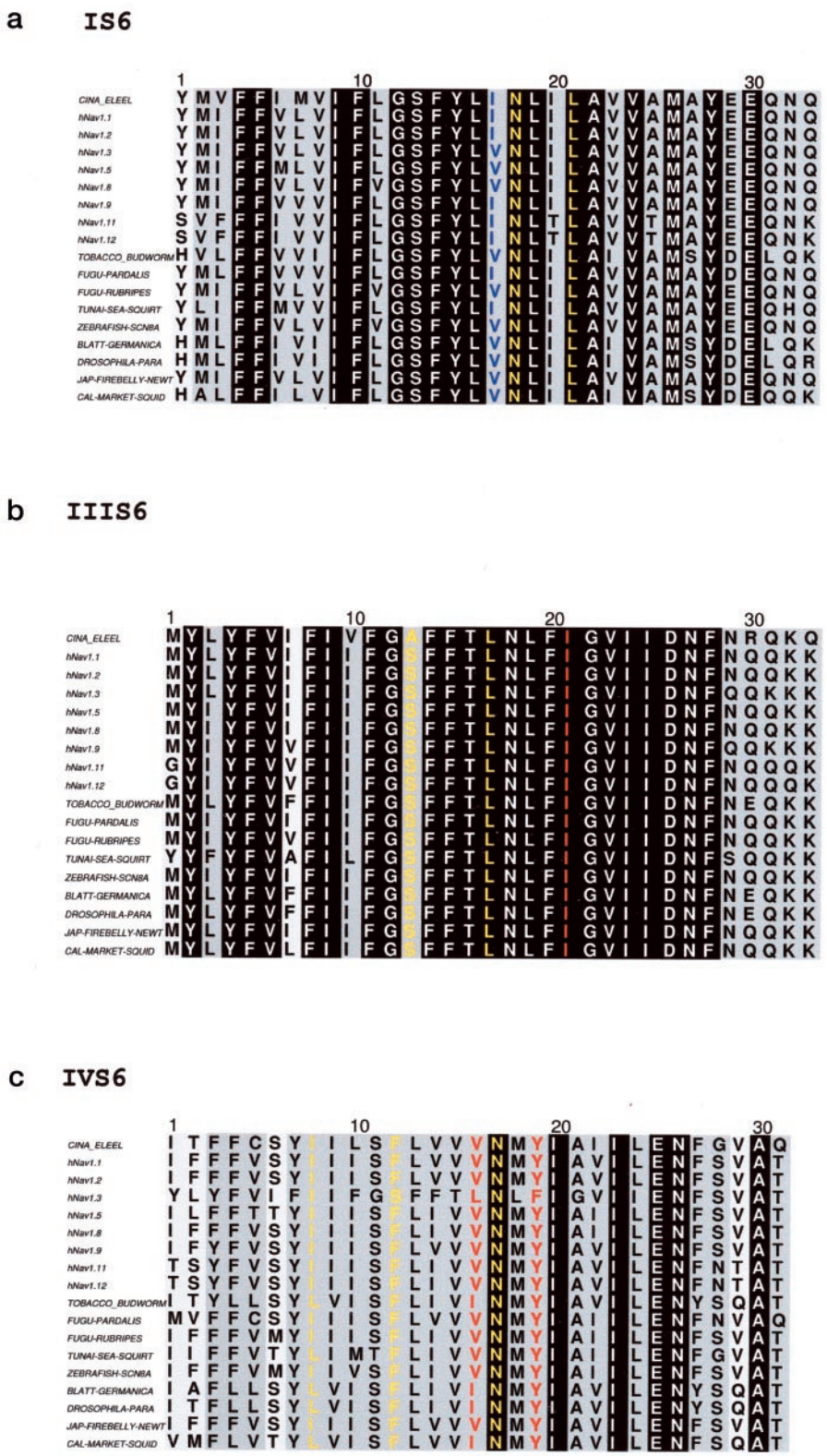

FIG. 1. **Sequence alignment of residues of the pore-forming S6 transmembrane segments of domains I, III, and IV, which have been identified as the binding sites for pharmacological agents.** Sodium channel sequences from a broad cross-section of species were aligned to illustrate sequence conservation in the pore including: the electric eel *E. electricus* (P02719); TTX-sensitive neuronal-expressed human sodium channels hNav1.1, hNav1.2, hNav1.3, and hNav1.12; TTX-resistant human heart hNav1.5, hNav1.8 expressed in neuroendocrine cells, and hNav1.11 expressed in dorsal root ganglion neurons; tobacco budworm *Heliothis virescens* (AF072493); the puffer fishes *Fugu pardalis* (AB030482) and *Fugu rubripes* (D37977); sea squirt *Halocynthia roretzi* (T43161); zebrafish *Danio rerio* (AF297658); german cockroach *Blattella germanica* (U73583); fruit fly *Drosophila melanogaster* (M32078); Japanese firebelly newt *Cynops pyrrhogaster* (AF123593); and California market squid *Loligo opalescens* (T43167). Totally conserved residues are shown in *black relief*, and highly conserved residues are in *gray relief*. Residues shown by site-directed mutagenesis to be critical for BTX binding are represented in *blue*, for lamotrigine binding in *red*, and for both BTX and lamotrigine in *yellow*.

ethanol concentration of 5%. Ethanol was added to the baselines in the same amount. An equivalent amount of ethanol was added to samples without ligand. Sodium channel samples with and without added ethanol produced identical CD spectra. Samples from several different preparations were examined with the same results.

Circular Dichroism Analyses—In the calculation of molar ellipticity, a mean residue mass of 114.5 daltons was used. The secondary structural analyses used DICHROWEB, an interactive webserver (31) that permits analyses via the following methods: SELCON3 (32), CONTIN (33, 34), CDSSTR (35), and K2D (36) with a wide range of protein spectral databases (all derived from soluble proteins (37)). The normalized root mean square deviation (NRMSD) parameter (38) was calculated as a measure of the quality of the fit of the calculated structure to the data. NRMSD values of <0.1 mean that the calculated and experimental spectra are in close agreement (39).

Modeling of the Sodium Channel and Its Interaction with LTG—Multiple sequence alignment of the S6 transmembrane residues from domains I, III, and IV was carried out using PSI-BLAST (40) and displayed using Alscript (41) (Fig. 1).

Homology modeling of S5, the P-loops, and S6 from all four domains used the open MthK channel x-ray structure (PDB accession number 1lnq) (42) as the framework, since LTG binds to the inactivated form of

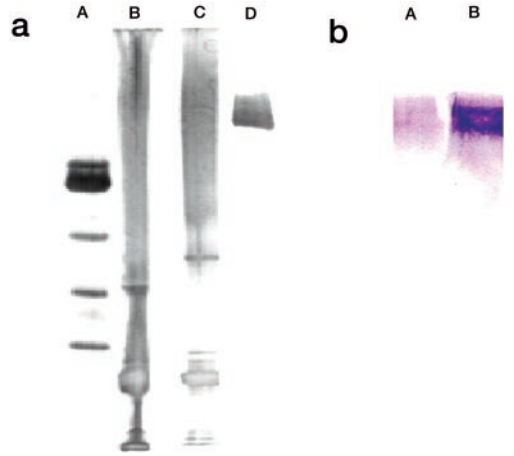

FIG. 2. **Purification of sodium channels.** *a*, SDS-PAGE of affinity-purified sodium channels. *Lane A*, molecular mass markers; *lane B* solubilized membranes; *lane C*, flow through of affinity column; *lane D*, purified sodium channels. *b*, Western blots. *lane A*, solubilized membranes; *lane B*, purified sodium channels.

the open channel. Areas of high homology between the sodium channel domains and potassium channel were aligned, *i.e.* S5 and S6 transmembrane segments based on both homology and secondary structure prediction. Non-homologous regions in the longer P-loops of domains I and III, which correspond to putative glycosylation sites, were deleted. The P-loops and N and C termini were modeled based on homologous segments of the KcsA channel structure (PDB accession number 1bl8).

Sodium channel sequences were aligned *versus* the MthK channel using ClustalW (43), and the structure was modeled employing the program Modeler 4 (44). Rigid-body minimization and simulated annealing of the model was carried out using the program CNS (45).

Docking studies between ligand and the channel model used the lamotrigine crystal structure (46) and the program AUTODOCK (47). The regions of close association between the docked lamotrigine and the sodium channel model were identified using the CCP4 (48) program CONTACT.

RESULTS

Purification of the Sodium Channel

The sodium channel from electric eel electroplax membranes was purified using procedures similar to those previously described (23, 24) but with the following modifications: the anti-sialic acid horse IgM affinity column was not eluted with colominic acid but instead was eluted with a KCl gradient as this resulted in higher yields and less degradation of the column, thus prolonging its useful lifetime. The presence of an enhanced mixture of protease inhibitors and the use of different buffers and detergent/lipid mixtures increased the yield and stability of the preparation. The eluted sodium channel was detected as a broad high molecular mass species on silver-stained gels (Fig. 2*a*) with an apparent molecular mass of ~280–300 kDa and identified by Western blot analyses with anti-α-2,8-*N*-acetylneuraminic acid horse IgM (Fig. 2*b*). The electroplax sodium channel is reported to consist of 30% by mass of carbohydrate, 12% sialic acid (9). Quantitative amino acid analyses were consistent with the reported sequence of the electroplax sodium channel (data not shown). Negative stain electron microscopy of the samples to be used for CD spectroscopy showed that they contained micelles, each consisting of a single protein with pseudo-4-fold symmetry and a central pore, as described earlier (16). Dynamic light scattering studies also showed the CD samples to be consistent with monomeric micellar species.[2]

[2] N. B. Cronin, unpublished results.

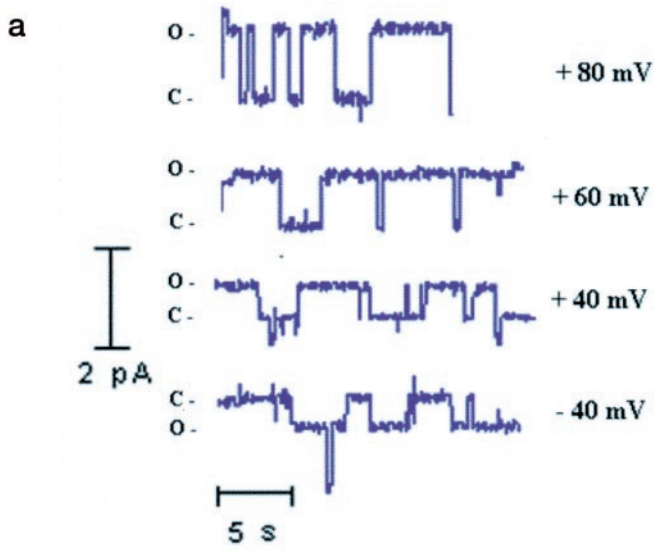

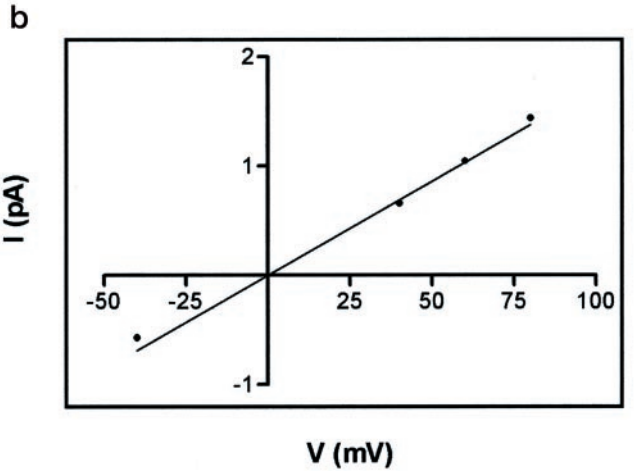

FIG. 3. **Electrophysiological characterization of purified sodium channels.** *a*, single-channel currents at different applied voltages of BTX-activated sodium channel in a tip-dip bilayer (electrolyte 0.5 M NaCl, 10 mM HEPES, pH 7.4). *b*, current/voltage curve plotted using the values obtained in *a*. The slope of the best-fit line gives a conductance value of ~17.5 pS.

Functional Characterization of the Sodium Channel

To demonstrate that the sodium channel retained functionality after purification and reconstitution, single channel conductance experiments in planar lipid bilayers were carried in the presence of BTX (Fig. 3*a*). BTX was used to remove the fast inactivation process, thus allowing single-channel events to be recorded with applied steady-state voltages. The single-channel conductance of 17.5 pS from the I–V plot (Fig. 3*b*) is within the range of values published from similar studies on the sodium channel (*e.g.* Ref. 49–51). The identity and functionality of the channel under investigation was confirmed by tetrodotoxin (TTX) block using 1 μM on both sides.

Structural Characterization of the Sodium Channel

CD Spectroscopy of Native Sodium Channels—CD spectroscopy was used to examine the secondary structure of the purified sodium channel protein. CD spectra of membrane proteins in lipid bilayers are subject to distortions due to optical artifacts such as differential light scattering and absorption flattening (29). To avoid these effects, the CD spectra of the sodium

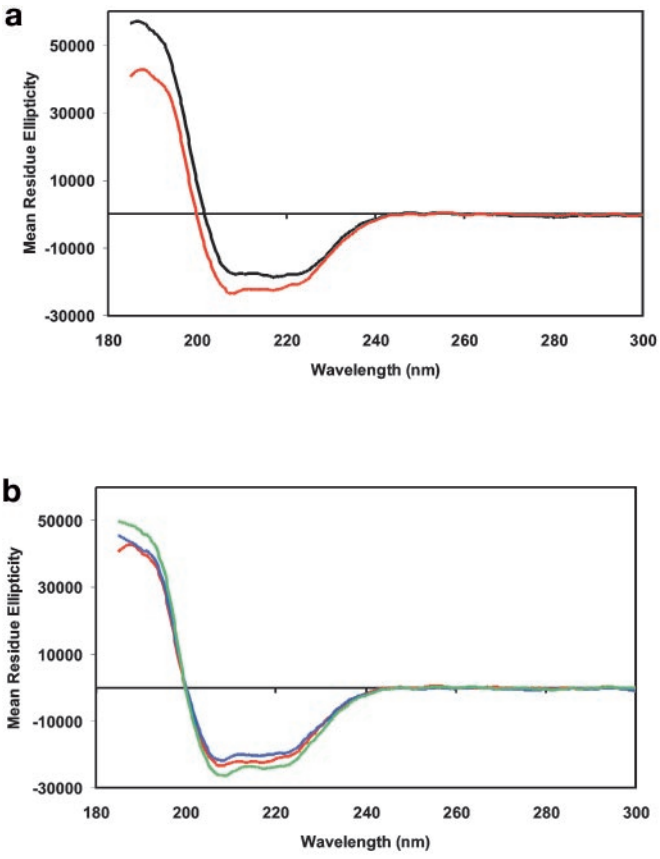

FIG. 4. **Circular dichroism spectra of (*a*) purified sodium channels (0.53 μM) with no ligand present (*black*) and in the presence of lamotrigine (*red*) and (*b*) in the presence of lamotrigine (*red*), batrachotoxin (*blue*), or with both lamotrigine and batrachotoxin (*green*).**

channel were measured in lipid/detergent mixed micelles, where such effects are negligible (52).

The native sodium channel gives rise to a spectrum that is characteristic of a protein with a high α-helical content, having peaks at ~221, 208, and ≤190 nm and a zero cross-over near 200 nm (Fig. 4*a*). Secondary structural analyses were performed for all spectra using a range of algorithms and reference databases derived from soluble proteins (31). The analysis program CDSSTR (with reference database 3) consistently produced the closest correspondence between experimental data sets and calculated spectra (based on NRMSD values), so its results are reported here: an α-helix content of 55% (Table I). However, virtually identical results were found for all methods tested. Indeed, nine different combinations of algorithms and reference data bases produced solutions with n.r.m.s.d. values of ≤0.1. The average value of the helix content from all these was 56%; this high correspondence of results obtained by different methods increases our confidence level in the veracity of the calculated values.

As a precaution, however, although the NRMSD values indicate a good correspondence between the calculated secondary structures and the actual structures, CD as a technique is most accurate in determining helix content. As a result, in this paper, discussions of the secondary structures will concentrate on the helix content of the protein. Furthermore, the interpretation of the analyses must bear in mind that all the reference data sets used in the analyses are derived from soluble proteins as they are the only ones currently available. Since the CD spectra of membrane proteins tend to have slightly different spectral characteristics (53), this could lead to some inaccuracy in the absolute values of the secondary structures calculated, although the changes in secondary structures measured will, in general, be unaffected.

TABLE I
Calculated secondary structures

Sample	% Secondary Structure				NRMSD[a]
	Helix	Sheet	Turn	Other	
Native	55	19	6	20	0.002
Native + LTG	64	10	6	19	0.005
Native + BTX	61	14	6	19	0.005
Native + both	68	12	4	15	0.003

[a] NRMSD is the parameter reflecting the goodness-of-fit between the calculated secondary structure and the experimental data.

Based on identification of helical transmembrane segments using hydropathy analyses for transmembrane segments S1–S4 in all the domains (~340 amino acids), analogy to the KcsA potassium channel structure for the region from S5 to S6 (~300 amino acids) (54), and analogy to the helical C-terminal domain of the human cardiac sodium channel consisting of ~80 amino acids (12), the minimum α-helical content is estimated to be 720 residues, or 40% helical. The measured value in this study is 55%, thus suggesting that the sodium channel contains additional helical structures beyond those in the thus-far identified helical regions.

CD Spectroscopy of Lamotrigine Binding to the Sodium Channel—A large molar excess (120×) of LTG was added to the native sample to fully shift the equilibrium toward the conformation associated with the open inactivated state since in proteoliposomes the electrical membrane potential difference is zero. LTG itself does not give rise to a CD signal over the wavelength range examined. The spectral changes observed in the protein involved an increase in magnitudes of the peaks at 221 and 208 nm and a change in ratio between the 190 and 221 nm peaks. This type of spectral change is indicative of an increase in helix content, which was born out by the secondary structural calculations (Table I).

The increase in helical content was calculated to be ~9%, or as many as 160 amino acids. Thus binding to the helical regions of the S6 segments (19) appears to induce increased order in other parts of the structure, perhaps to the P-regions, which are partially helical, or in the III–IV loop region, which NMR studies on an isolated fragment (11) suggest has a propensity for helix formation. Large tertiary structural changes, but only small changes in secondary structure, have been detected between the crystal structures of open and closed bacterial potassium channels (42, 55). However, secondary structural changes involving the III–IV loop region, which induces fast inactivation and is thought to enter the inner mouth of the channel under these conditions would not have been detected in the KcsA channel, which only contains the S5-P-S6 regions. In addition, regulation in eukaryote sodium channels is expected to be somewhat different than that for the bacterial potassium channels since the sodium channels contain loop regions connecting homologous domains in the pseudotetramer instead of individual monomers, as in the homotetramer of the KscA channel.

To eliminate the possibility of changes resulting from nonspecific protein-drug interactions, CD spectra were collected for the flow-through fraction from electroplax membranes after affinity purification of the sodium channel, which contained other membrane proteins but no detectable sodium channel, with and without a similar amount of lamotrigine added. The spectra for the flow-through and the flow-through plus lamotrigine were identical (data not shown).

CD Spectroscopy of Batrachotoxin Binding to the Sodium Channel—A 4-fold molar excess of BTX was used in the CD studies. The concentrations of BTX and sodium channel protein used were approximately the same as those used in the elec-

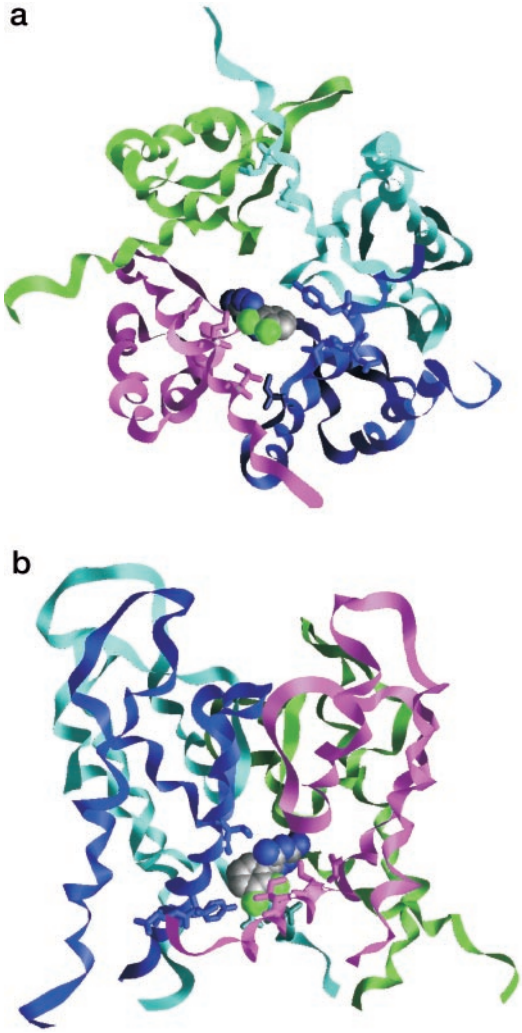

FIG. 5. **Model of the sodium channel comprised of the transmembrane S5-S6 and P-loop segments of domains I (*cyan*), II (*green*), III (*magenta*), and IV (*blue*) displayed as a backbone ribbon model with the lamotrigine-binding residues (as indicated from the mutational studies) depicted in stick representation.** The *topview* (*a*) shows the pseudo-4-fold symmetry about the central pore. Lamotrigine is depicted in a space-filling model with carbon atoms in *gray*, nitrogens in *blue*, and chlorines in *green*. Its optimal position, as defined by the AUTODOCK program, lies in the center of the pore, near the S6 helices of domains III and IV. The *sideview* (*b*) shows that the mutationally defined binding residues lie along one face of the S6 helices, lining the pore, and that the contact region of the docked ligand involves these same residues from domains III and IV. This figure was created using GRASP (71) software.

trophysiology experiments and sufficient to cause steady-state activation of purified sodium channel reconstituted into planar lipid bilayers, *i.e.* the channels can be triggered to fluctuate between open and closed states under applied steady-state or continuous voltages.

As was found in the LTG experiments, upon BTX binding the CD spectrum exhibited an increase in both the minima at 221 and 208 nm (Fig. 4*b*). The calculated secondary structure (Table I) indicated an increase (~6%) in α-helix content similar to, but somewhat smaller than, the LTG effect. The differences between the LTG and the BTX spectra are greater than the standard deviations of the measurements, so the structures formed in the presence of LTG and BTX are not identical. This is expected as they bind to different forms, inactivated and activated, respectively, of the open channel.

Binding of both LTG and BTX—It has been shown that BTX and sodium channel-blocking drugs bind with adjacent over-

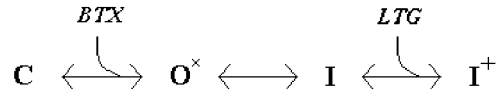

FIG. 6. **Schematic diagram showing different states of the sodium channel and the sites of influence of LTG and BTX.** O^x designates an open form with BTX bound, and I^+ is an inactivated form with LTG bound.

lapping but non-identical sites in IVS6 (56), IIIS6 (19, 57), IIS56 (58), and IS6 (59) transmembrane segments (Fig. 1). In addition, higher concentrations of local anesthetics can block sodium channels activated by BTX without displacing BTX (60). CD data were collected for the native channel in the presence of both LTG and BTX (Fig. 4*b*). The spectral changes observed in the 221 and 208 peaks upon binding both the toxin and the drug were larger than for either alone, and there is an apparent 13% increase in α-helical conformation (larger than either alone) (Table I). Thus it appears that there may be a further augmentation and stabilization of helical structure on binding of both BTX and LTG to the S6 segments of the inner pore of the sodium channel.

Model of the Sodium Channel Pore and Its Interactions with LTG and BTX

A molecular model that could be used to investigate the molecular nature of the binding of LTG in the pore was created by aligning residues 19–98, *i.e.* the pore-forming residues of the x-ray structure of the open form of a bacterial potassium channel, with residues 238–408 of domain I, residues 691–797 of domain II, residues 1127–1270 of domain III, and residues 1447–1547 of domain IV of the sodium channel. Residues 23–119 of the KcsA potassium channel x-ray structure were also used to model the P-loop regions and the N- and C-terminal residues of these segments. The orientations of the four domains were modeled by aligning domains I–IV of the sodium channel with chains A–D of the MthK structure in a clockwise arrangement as viewed from the extracellular surface (61). Residues forming the binding sites for LTG (as identified by mutational studies) all appear to lie on the pore-facing side of the S6 helices from domains I, III, and IV (Fig. 5).

The crystal coordinates for lamotrigine (46) were docked into this model using the program AUTODOCK. The highest ranking docked position has a final energy of −4.29 kcal/mol and on analysis gave consistent results with respect to the mutation studies. In the docked position, residues A1252 and L1256 of IIIS6, identified as the putative binding site lamotrigine by the mutation studies, make van der Waals contacts mainly with the triazine ring structure of lamotrigine and also one of the chlorine atoms of the dichlorophenyl ring structure, while F1555 and V1559 of IVS6, also identified by mutation studies as contributing to a lamotrigine binding site, make contacts chiefly with the dichlorophenyl ring.

DISCUSSION

Many drugs including local anesthetic compounds and anticonvulsant drugs such as lamotrigine block sodium channels in a voltage-dependent manner (19). When membranes are hyperpolarized block is minimal, but depolarization induces significant block. Lamotrigine blocks the channel (Fig. 6) in a use/frequency-dependent manner (62) and was found to block sustained repetitive firing of sodium-dependent action potentials in mouse spinal cord cultured neurons (63) and hence is used in the treatment of seizures. It has been proposed that use dependence arises from preferential binding to the inactivation states, which develop in response to rapid repetitive opening (62). However, although lamotrigine may bind with different affinities in a concentration-dependent manner to several dis-

crete dynamic states of the sodium channel, in this study only overall binding was explored in the absence of any applied membrane potential. Wild-type rat brain sodium channels have been shown to be inhibited by lamotrigine with a dissociation constant ranging from 12 to 32 μM (62, 64), *i.e.* in the same range as is required for the treatment of epilepsy in humans (63). The 50 μM used in these studies mimics these pharmacological and therapeutic concentrations.

Batrachotoxin is a lipid-soluble alkaloid that also binds specifically to sodium channels in a state-dependent manner (21) (Fig. 6). The main effects of BTX binding are a shift in the voltage dependence of activation in a hyperpolarizing direction, allowing steady-state activation of the channel, the inhibition of both fast and slow inactivation, and a small increased single-channel conductance coupled with a slightly altered ion selectivity (49). BTX in the micromolar concentration range causes steady-state activation of purified sodium channels reconstituted in phospholipid vesicles. A number of previous studies reported the electrical properties of BTX-modified *E. electricus* sodium channels in planar lipid bilayers. Single channel conductances of 15–25 pS were measured in various planar lipid bilayer systems (electrolyte: 0.5 M NaCl) (49–51). In the current study, a single-channel conductance of ~17–18 pS was measured in solvent-free, negatively charged lipid bilayers formed at a patch pipette tip (Fig. 3*a*). BTX was incorporated into vesicles containing sodium channels in the absence of a membrane potential. For the CD studies in mixed micelles, the sodium channels are not subjected to any membrane potential; therefore it was anticipated that BTX binding would stabilize the open conformation or one of the conformational transitions accompanying formation of the activated state.

In this study we examined conformational changes associated with formation of open states of the channel and found that the helix content increased dramatically. These conformational changes could involve the S6 segments, the P-regions, which form the outer pore and selectivity filter (although not exclusively as a recent study suggests (65)), or the III–IV cytoplasmic linker and the C terminus, which are involved in inactivation processes. BTX and LTG have been shown to have distinct and overlapping molecular determinants for binding in the inner pore. The common sites for state-dependent binding are residues on the same face of the IS6, IIIS6, and IVS6 helices (Fig. 5) (19). The structure of the KcsA channel (54) has established an α-helical architecture for the inner pore, which is assumed to be present in all members of the family of homologous ion channels (66) including by analogy the S6 segments of the sodium channel. These S6 transmembrane segments are thought to rotate during channel activation leading to local changes in side-chain interactions with contiguous transmembrane helices (67). Of the three S6 segments involved in binding, IIIS6 appears to be the most highly conserved and IVS6 shows the highest sequence variation (Fig. 1). However, in all three S6 segments, the residues identified as forming the drug binding site are all highly conserved, predominantly hydrophobic, and demonstrate a marked periodicity of every three to four residues across a large spectrum of species. Furthermore, mutations to alanine of two residues, Leu-1465 and Ile-1469 of the rat brain IIA sodium channel (corresponding to Leu-17 and Ile-21 of IIS6 in Fig. 1) both decreased lamotrigine binding and caused a positive shift in the steady-state activation curve (19). These residues, which contribute to stabilizing the open state, are all disposed along one face of the inner pore helix and are proposed to face the lumen of the pore in the activated and inactivated open states of the channel (Fig. 5).

CD analyses of the KcsA channel performed over a range of different pH values to induce a conformational change (67) indicated that there was no significant change in secondary structure. This suggested that pH-dependent channel opening must be coupled to the motion of entire domains or secondary structure elements in this truncated channel. An analysis of the voltage-gated potassium channel using cysteine modifications of the S6 segment led to the conclusion that the presence of a Pro-*X*-Pro motif in these helices would give rise to a 'bent S6′ helix model as a variation on the KcsA model (68). The voltage-gated sodium channel S6 segments do not have this motif, but the presence of conserved glycines in three of four of these helices can lead to the proposal that the inner and outer parts of S6 segments could move independently during activation gating. However, rigid body movements of S6 segments are unlikely to be the source of the observed spectral changes, which clearly result from secondary structure conformational changes.

Other possible sources for the observed conformational change are the P-loops or the III–IV linker responsible for inactivation. There is evidence for conformational flexibility in the P-loops. Indeed, investigation of the Drk1 K channel identified subconductance states relating to incomplete channel opening due to incomplete pore formation (69). Mutant *Shaker* K^+ channels allowed recording of these subconductance states suggesting the existence of different conformations of the selectivity filter reflecting incomplete pore formation giving rise to distinct conductance rates. In contrast to this result, spin labeling experiments on the non-voltage-gated KcsA K^+ channel led to the conclusion that the selectivity filter remained immobile during gating (67). Finally, mutagenesis data has implicated the S4-S5 intracellular linker of domain IV in the sodium channel as the probable receptor for the inactivation particle (70). In the current work, the simultaneous addition of LTG and BTX suggests binding to the open inactivated state so the observed secondary structure change could involve conformational changes associated with inactivation particle binding.

On the bases of the CD spectral changes observed in the present study, we propose a model for activation and inactivation that involves a significant secondary structural conformation change in addition to the rigid body movements of the S6 transmembrane helices previously inferred. This is likely to involve the inner pore helices, P regions, and the III–IV interdomain linker.

Acknowledgments—We thank Peter Sherritt of the Protein and Nucleic Acid Chemistry Facility at the University of Cambridge for the quantitative amino acid analyses, Dr. Robert W. Janes of Queen Mary College, University of London for lamotrigine, Dr. R. Schneerson of the National Institutes of Health for the horse antiserum, Dr. J. W. Daly of the National Institutes of Health for batrachotoxin, and Dr. Ulrich Gohlke, Birkbeck College, University of London for help with the electron microscopy. H. D. acknowledges advice and comments by Dr. S. Bendahhou (Institut de Pharmacologie Moléculaire et Cellulaire, CNRS, Sophia-Antipolis, France) and thanks Dr. J. Dempster of Strathclyde University (Glasgow, UK) for free electrophysiology acquisition and analysis software.

REFERENCES

1. Hille, B. (2001) *Ionic Channels of Excitable Membranes.* 3rd Ed., Sinauer, Sunderland, MA
2. Balser, J. R. (2001) *J. Mol. Cell Cardiol.* **33,** 599–613
3. Lehmann-Horn, F., and Jurkat-Rott, K. (1999) *Physiol. Rev.* **79,** 1317–1372
4. Ptáček L. J., and Bendahhou, S. (2001) *Disorders of Voluntary Muscle*, 7th Ed., pp. 604–634, Cambridge University Press, Cambridge
5. Keynes, R. D. (2001) *Novartis Found. Symp.* **241,** 5–14
6. Bezanilla, F. (2000) *Physiol. Rev.* **80,** 555–592
7. Goldin, A. L., Barchi, R. L., Caldwell, J. H., Hofmann, F., Howe, J. R., Hunter, J. C., Kallen, R. G., Mandel, G., Meisler, M. H., Netter, Y. B., Noda, M., Tamkun, M. M., Waxman, S. G., Wood, J. N., and Catterall, W. A. (2000) *Neuron* **28,** 365–368
8. Noda, M., Shimizu, S., Tanabe, T., Takai, T., Kayano, T., Ikeda, T., Takahashi, H., Nakayama, H., Kanaoka, Y., Minamino, N., Kangawa, K., Matsuo, H., Raftery, M. A., Hirose, T., Inayama, S., Hayashida, H., Miyata, T., and Numa, S. (1984) *Nature* **312,** 121–127
9. Levinson, S. R., Thornhill, W. B., Duch, D. S., Recio-Pinto, E., and Urban,

B. W. (1990) in *Ion Channels* (Narahashi, T., ed.) Vol. 2, pp. 33–64, Plenum Publishing Corp., New York
10. Patton, D. E., West, J. W., Catterall, W. A., Goldin, A. L. (1992) *Proc. Natl. Acad. Sci. (U. S. A.)* **89,** 10905–10909
11. Kuroda, Y., Maeda, Y., Miyamoto, K., Tanaka, K., Kanaori, K., Otaka, A., Fujii, N., and Nakagawa, T. (1999) *Biophys. J.* **77,** 1363–1373
12. Cormier, J. W., Rivolta, I., Tateyama, M., Yang, A.-S., and Kass, R. S. (2002) *J. Biol. Chem.* **277,** 9233–9241
13. Zhang, H., Kolibal, S., Vanderkooi, J. M., Cohen, S. A., and Kallen, R. G. (2000) *Biochim. Biophys. Acta* **1467,** 406–418
14. Stuhmer, W., Conti, F., Suzuki, H., Wang, X. D., Noda, M., Yahagi, N., Kubo, H., and Numa, S. (1989) *Nature* **339,** 597–603
15. Heinemann, S. H., Schlief, T., Mori, Y., and Imoto, K. (1994) *Braz. J. Med. Biol. Res.* **27,** 2781–2802
16. Sato, C., Ueno, Y., Asai, K., Takahashi, K., Sato, M., Engel, A., and Fujiyoshi, Y. (2001) *Nature* **409,** 1047–1051
17. Patten, C. D., Caprini, M., Planells-Cases, R., and Montal, M. (1999) *FEBS Lett.* **463,** 375–381
18. Anger, T., Madge, D. J., Mulla, M., and Riddall D. (2001) *J. Med. Chem.* **44,** 115–137
19. Yarov-Yarovoy, V., Brown, J., Sharp, E. M., Clare, J. J., Scheuer, T., and Catterall, W. A. (2001) *J. Biol. Chem.* **276,** 20–27
20. Narahashi, T. (1986) *Ann. N. Y. Acad. Sci.* **479,** 133–151
21. Vedantham, V., and Cannon, S. C. (2000) *Biophys. J.* **78,** 2943–2958
22. Allen, P. Z., Glode, M., Schneerson, R., and Robbins, J. B. (1982) *J. Clin. Microbiol.* **15,** 324–329
23. Miller, J. A., Agnew, W. S., and Levinson, S. R. (1983) *Biochemistry* **22,** 462–470
24. James, W. M., Emerick, M. C., and Agnew, W. S. (1989) *Biochemistry* **28,** 6001–6009
25. Laemmli, U. K. (1970) *Nature* **227,** 680–685
26. Merril, C. R., Goldman, D., Sedman, S. A., and Ebert, M. H. (1981) *Science* **211,** 1437–1438
27. Smith, P. K., Krohn, R. I., Hermanson, G. T., Mallia, A. K., Gartner, F. H., Provenzano, M. D., Fujimoto, E. K., Goeke, N. M., Olson, B. J., and Klenk, D. C. (1985) *Anal. Biochem.* **150,** 76–85
28. Hanke, W., Methfessel, C., Wilmsen, G., and Boheim, G. (1984) *Biochem. Bioenerg. J.* **12,** 329–339
29. Wallace, B. A., and Mao, D. (1984) *Anal. Biochem.* **142,** 317–328
30. Savitsky, A., and Golay, M. J. E. (1964) *Anal. Chem.* **36,** 1627–1639
31. Lobley, A., Whitmore, L., and Wallace, B. A. (2002) *Bioinformatics* **18,** 211–212
32. Sreerama, N., Venyaminov, S. Y., and Woody, R. W. (1999) *Prot. Science* **8,** 370–380
33. Provencher, S. W., and Glockner, J. (1981) *Biochemistry* **20,** 33–37
34. vanStokkum, I. H. M., Spoelder, H. J. W., Bloemendal, M., vanGrondelle, R., and Groen, F. C. A. (1990) *Anal. Biochem.* **191,** 110–118
35. Sreerama, N., and Woody, R. W. (2000) *Anal. Biochem.* **282,** 252–260
36. Andrade, M. A., Chacón, P., Merelo, J. J., and Morán, F. (1993) *Protein Eng.* **6,** 383–390
37. Sreerama, N., Venyaminov, S. Y., and Woody, R. W. (2000) *Anal. Biochem.* **287,** 243–251
38. Wallace, B. A., and Teeters, C. L. (1987) *Biochemistry* **26,** 65–70
39. Brahms, S., and Brahms, J. (1980) *J. Mol. Biol.* **138,** 149–178
40. Altschul, S. F., Madden, T. L., Schaffer, A. A., Zhang, J., Zhang, Z., Miller, W., and Lipman, D. J. (1997) *Nucleic Acids Res.* **25,** 3389–3402
41. Barton, G. J. (1993) *Protein Eng.* **6,** 37–40
42. Jiang, Y. X., Lee, A., Chen, J. Y., Cadene, M., Chait, B. T., and MacKinnon, R. (2002) *Nature* **417,** 523–526
43. Thompson, J. D., Higgins, D. G., and Gibson, T. J. (1994) *Nucleic Acids Res.* **22,** 4673–4680
44. Šali, A., and Blundell T. L. (1993) *J. Mol. Biol.* **234,** 779–815
45. Brunger, A. T., Adams, P. D., Clore, G. M., Delano, W. L., Gros, P., Grosse-Kunstleve, R. W., Jiang, J.-S., Kuszewski, J., Nilges, M., Pannu, N. S., Read, R. J., Rice, L. M., Simonson, T., and Warren G. L. (1998) *Acta Crystallogr. Sect. D Biol. Crystallogr.* **54,** 904–921
46. Janes, R. W., Lisgarten, J. N., and Palmer, R. A. (1989) *Acta Crystallogr. Sect. C Cryst. Struct. Commu.* **45,** 129–132
47. Goodsell, D. S., Morris, G. M., and Olsen, A. J. (1996) *J. Mol. Recognit.* **9,** 1–5
48. Collaborative Computational Project: Number 4 (1994) *Acta Crystallogr. Sect. D Biol. Crystallogr.* **50,** 760–763
49. Recio-Pinto, E., Duch, D. S., Levinson, S. R., and Urban, B. W. (1987) *J. Gen. Physiol.* **90,** 375–395
50. Bendahhou, S., Thoiron, B., and Duclohier, H. (1991) *C. R. Acad. Sci.* (*Paris*) **312,** 277–284
51. Wartenberg, H. C. Wartenberg, J. P., and Urban, B. W. (2001) *Basic Res. Cardiol.* **96,** 645–651
52. Mao, D., and Wallace, B. A. (1984) *Biochemistry* **23,** 2667–2673
53. Chen, Y., and Wallace, B. A. (1997) *Biophys. Chem.* **65,** 65–74
54. Doyle, D. A., Morais-Cabral, J. H., Pfuetzner, R. A., Kuo, A. L., Gulbis, J. M., Cohen, S. L., Chait, B. T., and MacKinnon, R. (1998) *Science* **280,** 69–77
55. Zhou, Y. F., Morais-Cabral, J. H., Kaufman, A., and MacKinnon, R. (2001) *Nature* **414,** 43–48
56. Wang, S. Y., and Wang, G. K. (1999) *Biophys. J.* **76,** 3141–3149
57. Wang, S. Y., Nau, C., and Wang, G. K. (2000) *Biophys. J.* **79,** 1379–1387
58. Wang, S. Y., Barile, M., and Wang, G. K. (2001) *Mol. Pharmacol.* **59,** 1100–1107
59. Wang, S. Y., and Wang, G. K. (1998) *Proc. Natl. Acad. Sci. (U. S. A.)* **95,** 2653–2658
60. Narahashi, T. (1999) *Adv. Neurol.* **79,** 457–480
61. Li, R. A., Ennis, I. L, French, R. J., Dudley, S. Jr., Tomaselli, G. F., and Marban, E. (2001) *J. Biol. Chem.* **276,** 11072–11077
62. Koorsgaard, M. P. G., Christophersen, P., Ahring, P. K., and Olesen, S.-P. (2001) *Pflügers Arch. Eur. J. Physiol.* **443,** 18–30
63. Otoom, S. A., and Nusier, M. K. (2001) *Cytobios* **106,** Suppl**. 1,** 75–83,
64. Xie, X., Lancaster, B., Peakman, T., and Garthwaite, J. (1995) *Pflügers Arch. Eur. J. Physiol.* **430,** 437–446
65. Chen, Z., Alcayaga, C., Suarez-Isla, B. A., O'Rourke, B., Tomaselli, G., and Marban, E. (2002) *J. Biol. Chem.* **277,** 24653–24658
66. Hanlon, M. R., and Wallace, B. A. (2002) *Biochemistry* **41,** 2886–2894
67. Perozo, E., Cortes, D. M., and Cuello, L. G. (1999) *Science* **285,** 73–78
68. del Camino, D., Holmgren, M., Liu, Y., and Yellen, G. (2000) *Nature* **403,** 321–325
69. Chapman, M. L., VanDongen, H. M. A, and VanDongen, A. M. J. (1997) *Biophys. J.* **72,** 708–719
70. McPhee, J. C., Ragsdale, D. S., Scheuer, T., and Catterall, W. A. (1998) *J. Biol. Chem.* **273,** 1121–1129
71. Nicholls, A., Sharp, K. A., and Honig, B. (1991) *Proteins* **11,** 281–296